Mechanics Research Communications 81 (2017) 11–16

Contents lists available at ScienceDirect

Mechanics Research Communications

journal homepage: www.elsevier.com/locate/mechrescom

Damping in a parametric pendulum with a view on energy harvesting

Franco E. Dotti[a,*], Florencia Reguera[b], Sebastián P. Machado[a]

[a] Grupo de Investigación en Multifísica Aplicada (GIMAP), Universidad Tecnológica Nacional, Facultad Regional Bahía Blanca, Consejo Nacional de Investigaciones Científicas y Técnicas, Argentina
[b] Grupo de Investigación en Multifísica Aplicada (GIMAP), Universidad Tecnológica Nacional, Facultad Regional Bahía Blanca, Consejo Nacional de Investigaciones Científicas y Técnicas, Departamento de Ingeniería, Universidad Nacional del Sur, Argentina

ARTICLE INFO

Article history:
Received 13 December 2016
Accepted 11 February 2017

Keywords:
Energy harvesting
Parametric pendulum
Damping
Optimization

ABSTRACT

The present article addresses the quantification of damping in a parametric pendulum, with a view on further applications in the design of energy harvesting devices. Detailed new experimental data is obtained for such purpose, and a novel mathematical model is presented. Linear and quadratic viscous damping and also dry friction are taken into account. To introduce the dry friction component, the pendulum axis is mounted on ball bearings. This is considered as a very realistic situation of a harvester. Damping parameters are determined by minimizing the difference between numerical and experimental time histories. It is shown that the damping model here presented is more adequate to replicate experiments than commonly used linear models, which consider only a linear viscous damping term characterized by means of free decay tests. It is also pointed that linear models are not adequate for refined studies, since they can lead to erroneous predictions of rotation zones, and consequently to wrong considerations in the design of pendulum harvesters.

1. Introduction

The growing global interest in clean energy has allowed the development of many technologies aimed at energy harvesting from ambient vibrations. This trend has led to review some well-known mechanical systems in the search for suitable harvesting devices. Based on the high kinetic energy available in its rotational motion, the parametric pendulum is one of those systems recently revisited [1–6]. The basic idea of the harvester consists of a pendulum with a vertical motion induced by an ambient energy source. If stable rotations are achieved, a generator attached to the pendulum axis may extract electrical energy. Two sources of ambient vibrations are mainly thought as external excitation: one is the motion of the sea waves, of stochastic nature; and the other is given by the motion of steady vibrating machines, which is generally harmonic and thus easily predictable. This predictability can be used in the design of the pendulum harvester to improve its ability of achieving rotations [7,8].

Damping is an important variable in the design of mechanical harvesters due to its close relation with energy consumption and consequently with efficiency of the system. In fact, it has been pointed out that energy cannot be extracted from a pendulum if damping is very high [2]. It is common practice to assume a damping force due to air drag, which is defined as proportional to the tangential velocity of the bob [2–11]. The proportionality constant of this linear model is usually estimated from a free decay test, assuming an exponential decay of amplitude. This choice is attractive because of its mathematical simplicity, but it is known since a long time that linear damping often cannot represent accurately the behavior of real pendulums [12–14]. This happens mainly because a real pendulum involves sliding or rolling surfaces, such as ball bearings, where Coulomb's nonlinear dry friction cannot be neglected [13]. Besides, if the motion of the pendulum happens at a high Reynolds number, viscous friction may include a quadratic term [13,14] or it may even be purely quadratic [15].

Following those somewhat old but consistent ideas, we propose a mathematical model of the parametric pendulum. To account dry friction, the axis of rotation is assumed to be mounted on ball bearings. We consider this as a realistic situation for an energy harvester, since ball bearings have a good balance between cost, maintenance and friction [16,17]. Besides, linear and quadratic viscous friction terms are also taken into account. The model is derived and tested experimentally considering a reciprocating motion as a parametric excitation. This motion can be found in a wide range of industrial machines, including engines and pumps, where a crank-rod system is used to convert circular motion into linear motion or *vice versa*.

* Corresponding author.
E-mail address: fdotti@frbb.utn.edu.ar (F.E. Dotti).

http://dx.doi.org/10.1016/j.mechrescom.2017.02.009
0093-6413/

Nevertheless, the model here presented can be useful for any other excitation of harmonic or stochastic nature. The study is focused on rotational motion which is, as mentioned before, the desired steady state of the pendulum for energy harvesting purposes.

Damping parameters are identified by solving an optimization problem. Identification is based on the minimization of the mean error between experimental data and numerical calculations of the angular position of the pendulum bob. This technique is similar to that used in reference [18], named Fitting Time Histories.

The article is organized as follows. After this introduction (Section 1), we introduce the mathematical model (Section 2) and make a description of the experimental device (Section 3). Then the objective function of the optimization problem is obtained (Section 4). Finally, the results of the study are presented and discussed, focusing on a comparison with a linear damping model (Section 5).

2. Mathematical model

The governing differential equation of the parametrically excited pendulum can be set up by using Lagrange's equation for single-DOF non conservative systems. It is a second-order ordinary differential equation given by

$$ml^2\theta'' + T_v + T_C + ml\left(y'' + g\right)\sin\theta = 0, \tag{1}$$

where m is the mass of the pendulum bob, l the distance between the center of gravity and the axis of the pendulum, g the acceleration of gravity, y the vertical displacement of the axis, θ is the angle measured from the hanging position and T_v and T_C are respectively the viscous friction torque and the Coulomb's friction torque. Derivatives $(\bullet)'$ are performed with respect to time τ.

Let's consider the schematic pendulum-shaker system of Fig. 1. The connecting joint between rod and crank rotates at a constant angular velocity Ω, following a circumferential trajectory. Thus, the displacement of that joint projected horizontally or vertically is exactly sinusoidal in time. Now, the tilt angle of the rod is continuously varying during the cycle of motion. Therefore the linear motion of the upper end of the rod is more complex than a sine function. This linear motion, then transmitted to the pendulum axis, is given by

$$y = r\left(1 - \cos\Omega\tau\right) + L\left(1 - \sqrt{1 - \lambda^2\sin^2\Omega\tau}\right), \tag{2}$$

where r is the crank radius, L is the rod length and $\lambda = r/L$ is the crank/rod ratio.

To determine the viscous damping torque T_v, a drag force has to be established. It has been proposed that this force is neither linear nor quadratic in velocity, but rather a combination of the two [14]. Thus, it seems reasonable to define the drag force as $F_v = aV^2 + bV$, where V is the magnitude of the tangential velocity of the bob and a and b are constant coefficients. Being $V = l|\theta'|$ and $T_v = l\,F_v$, the viscous damping torque can be expressed as

$$T_v = a\,l^3\left(\theta'\right)^2 sgn\theta' + b\,l^2\theta'. \tag{3}$$

The sign function $\mathrm{sgn}\,\theta'$ is needed since both linear and quadratic damping must oppose motion.

The dry friction torque T_C is estimated according to elementary laws of friction, as proportional to the applied force [13,17,19,20]. Hence

$$T_C = \mu\, r_b F_N sgn\theta', \qquad F_N = |ml\left(\theta'\right)^2 + mg\cos\theta|, \tag{4}$$

where μ is the Coulomb friction coefficient, r_b is the bearing bore radius and F_N is the radial dynamic load on the bearings due to the pendulum motion. Since F_N is also the axial load of the pendulum rod, it is calculated by elementary mechanics considerations [21]. Dry friction also opposes motion, thus the sign function $sgn\theta'$ is also present.

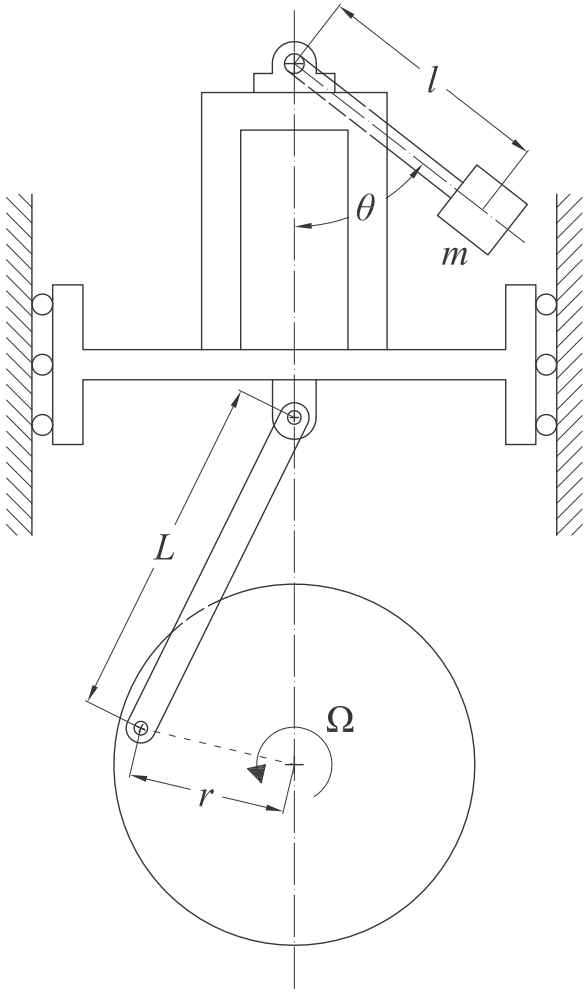

Fig. 1. Schematic pendulum-shaker system, with reciprocating parametric excitation.

Now, introducing Eqs. (2)–(4) into Eq. (1), the non-dimensional equation of motion of the system can be expressed as

$$\ddot{\theta} + \alpha\,\dot{\theta}^2 sgn\dot{\theta} + \beta\,\dot{\theta} + M|\dot{\theta}^2 + \cos\theta|sgn\dot{\theta} + \\ + \left(R\cos\omega t + \lambda^3 R\frac{\Lambda_3}{\Lambda_1^3} + \lambda R\frac{\Lambda_2}{\Lambda_1} + 1\right)\sin\theta = 0, \tag{5}$$

where the following definitions have been made

$$\omega_0 = \sqrt{\frac{g}{l}}, \quad t = \omega_0\tau, \quad \omega = \frac{\Omega}{\omega_0}, \quad R = \frac{r\omega^2}{l} \\ \alpha = \frac{a\,l}{m}, \quad \beta = \frac{b}{m\,\omega_0}, \quad M = \frac{\mu\, r_b}{l}, \\ \Lambda_1 = \sqrt{1 - \lambda^2\sin^2\omega t}, \quad \Lambda_2 = \cos^2\omega t - \sin^2\omega t, \\ \Lambda_3 = \cos^2\omega t \cdot \sin^2\omega t. \tag{6}$$

In Eq. (6), the superimposed dot means the derivative with respect to dimensionless time t. The magnitudes ω, R, α, β and M are non-dimensional parameters associated respectively to the forcing frequency, the forcing amplitude, quadratic viscous damping, linear viscous damping and dry friction. Depending on the settings of these five parameters along with λ, and the choice of initial conditions θ_0 and $\dot{\theta}_0$, several steady state solutions of Eq. (5) can be obtained, corresponding to different responses of the physical system [7,8]. The most common responses are the rest position, oscillations, rotations and chaotic motion.

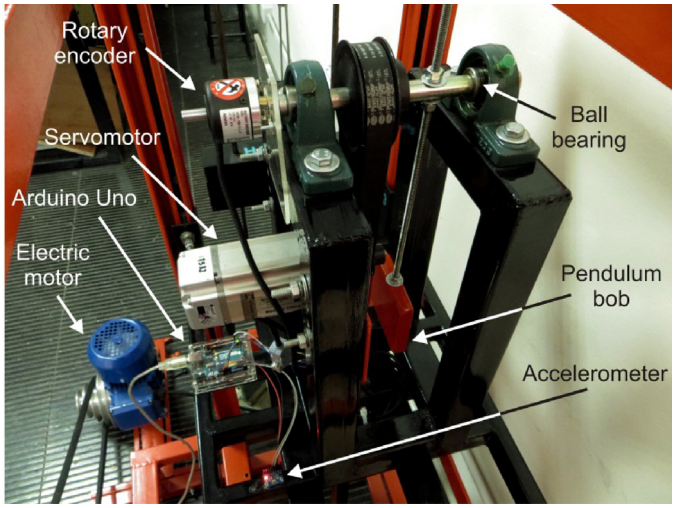

Fig. 2. Experimental device, mounted on a crank-rod mechanical shaker at the GIMAP laboratory.

3. Experimental setup

The experimental device consists of a pendulum mounted on a crank-rod mechanical shaker, as shown in Fig. 2. The rotatory motion of the shaker is produced by an electric gearmotor of 0.75 HP with a reducer pulley attached. A total of 15 experiments are allowed, with five possibilities for Ω: 2.36 Hz, 1.92 Hz, 1.54 Hz, 1.18 Hz and 0.87 Hz; and three possibilities for r: 205 mm, 106.5 mm and 72.5 mm. The rod of the shaker has a fixed length of $L = 575$ mm.

The pendulum device allows experiments for a wide range of Ω. Practical limits of the pendulum rod length are 170 mm $< l <$ 270 mm, thus natural frequency ω_0 can be varied from 6.028 to 7.596 Hz. The pendulum rod is attached to a shaft, which is in turn mounted on two P203 ball bearings ($r_b = 12.25$ mm) to the supporting frame. The shaft also has a gear-belt coupling with a servomotor, which is able to provide a control torque to the pendulum (not used in the present study). Two interchangeable masses can be used: $m = 0.745$ kg and $m = 1.460$ kg. The dimensions are similar to those of the experimental device of reference [4].

Each experiment is started manually by the operator. Once the pendulum is already in motion, the shaker is turned on and the initial time is set at the first positive peak of the measured acceleration y''. This ensures no phase shift with respect to Eq. (2). The initial conditions θ_0 and $\dot{\theta}_0$ are then measured by the data acquisition system so their values are known, although they cannot be imposed exactly.

Data acquisition is performed by using relatively low cost components. The measurement of the pendulum angular position is performed by an Autonics E40H8-1024-6L5 incremental encoder attached to the pendulum axis. Meanwhile the imposed acceleration of the shaker is measured by an InvenSense MPU-6050 accelerometer placed on the shaker worktable. The signals from both the encoder and the accelerometer are collected by an Arduino Uno board and data is sent to a dedicated computer.

4. Identification of damping parameters

Physical parameters a, b and μ are determined by minimizing numerical and experimental time histories of θ [18]. But a, b and μ are not the only variables of the optimization problem: we include also as variables the initial conditions θ_0 and $\dot{\theta}_0$ of the several time histories employed. This must be done because of the dependence of nonlinear systems on initial conditions, and because of an uncertainty in the measurements of those initial conditions. Thus, we consider the following error function

$$E_\theta\left(a, b, \mu, \left(\theta_{0,j}, \dot{\theta}_{0,j}\right)_{j=1}^{N}\right) = \sum_{j=1}^{N}\sum_{k=1}^{n} |\hat{\theta}_{j,k} - \theta_j(t_k)|, \tag{7}$$

where $\hat{\theta}_{j,k}$ is an individual measurement of the angular position, corresponding to the time history j and measured at a time t_k. Besides, N is the total of time histories considered and $(t_n, \hat{\theta}_{j,n})$ is the last individual measurement of the time history j. Each simulated time history $\theta_j(t)$ is obtained as a numerical function by solving Eq. (5) for a given set of a, b and μ.

Now, although each experiment is performed until there is high certainty that the steady state is reached, t_k of Eq. (7) is generally much smaller than the total time of the experiment. This allows saving computational cost in the evaluation of the function E_θ. However, it is mandatory for the simulation to achieve the same steady state as the experiment. Thus, simulation is performed for a total time $t_{\text{sim}} > t_k$ and the response is checked. Then a "response number" n_r is evaluated, being $n_r = 1$ if the simulated steady state coincides with the experimental and $n_r = 0$ otherwise. Hence, the following optimization problem must be solved, where the objective function f_{obj} is a penalized version of the error E_θ

$$\min\left\{f_{\text{obj}}\left(a, b, \mu, \left(\theta_{0,j}, \dot{\theta}_{0,j}\right)_{j=1}^{N}\right) = \begin{cases} E_\theta, & \text{if } n_r = 1 \\ \kappa E_\theta, & \text{if } n_r = 0 \end{cases}\right\}. \tag{8}$$

The penalty factor κ is a high number chosen arbitrarily. Finding a minimum value of the objective function f_{obj} implies solving an optimization problem with $3 + 2N$ variables.

Once the optimal damping parameters are obtained, a validation with a new experimental time history is not direct. That is due, again, to the dependence on initial conditions. By fixing a, b and μ at the optimal values and solving Eq. (5), we would like to obtain a simulation which replicates the experiments. But this may not happen if the measured initial conditions are employed, due to the uncertainty mentioned above. Nevertheless, an adequate set of initial conditions *must be found* in a reduced neighborhood of the measurements. Hence, for every validation with a new time history, the optimization problem of Eq. (8) is solved again, now with a, b and μ fixed, and N=1. This reduces the number of variables to two: θ_0 and $\dot{\theta}_0$, also with a small search field, which jointly give a fast resolution problem.

5. Results and discussion

First we determine a, b and μ of the real system. As mentioned, the study is focused on rotations because of their main importance in energy harvesting. In fact, the problem of Eq. (8) is solved only with experiments producing rotations as steady states. Nevertheless, these rotations sometimes present chaotic transients [22], which are of course taken into account, and other responses as oscillations and equilibrium are considered to a lesser extent in the validation.

In the identification problem, a total of 14 experiments are employed, with an external excitation characterized by $r = 72.5$ mm and $\Omega = 1.54$ Hz. This corresponds to a favorable condition for rotations. To keep the experiments mutually comparable, they are all performed in the same lubrication and temperature conditions since these factors influence on damping estimation. In addition, adjustments between one experiment and other are reduced to the least possible, and mass of the bob and length of the rod are modified only once.

The numerical minimization of the objective function f_{obj} is addressed with respect to a, b and μ, and the initial condi-

Table 1
Results of the optimization calculations performed to determine the physical damping parameters a, b and μ.

Calc.	Experimental set					DE data		Best results			
	m (Kg)	l (mm)	R	ω	N	N_p	G	a (α)	b (β)	μ (M)	f_{obj}
#1	1.46	265	0.657	1.585	3	80	3001	0.000 (0.000)	0.525 (0.059)	0.157 (0.007)	124.73
#2	0.745	260	0.687	1.57	4	100	3031	0.001 (0.000)	0.473 (0.103)	0.145 (0.008)	2108.37
#3	0.745	260	0.687	1.57	8	180	1439	0.003 (0.001)	0.622 (0.136)	0.126 (0.006)	3948.37
#4	1.46	265	0.657	1.585	7	160	1730	0.002 (0.000)	0.509 (0.057)	0.135 (0.006)	3237.61
	0.745	260	0.687	1.57				0.002 (0.001)	0.509 (0.111)	0.135 (0.006)	

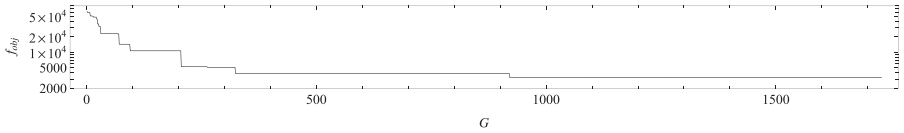

Fig. 3. Convergence plot for Calculation #4 (see Table 1). Fitness of the best individual of the population vs. number of generations G.

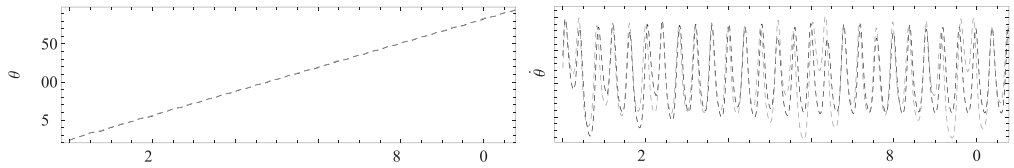

Fig. 4. Comparative plots of experimental and simulated angular position and velocity for $R = 0.696$, $\omega = 1.580$, $\lambda = 0.126$. (–): Experimental. (- -): Simulation A, $a = 0$ ($\alpha = 0$), $b = 0.5$ ($\beta = 0.109$), $\mu = 0.15$ ($M = 0.007$). (_ _): Simulation B, $a = 0$ ($\alpha = 0$), $b = 0.3$ ($\beta = 0.066$), $\mu = 0$ ($M = 0$).

tions, as stated in Eq. (8). A global optimization approach is used due to the multiple local minima of the problem. We opted for a proven method: a standard Differential Evolution algorithm (DE/rand/1/bin) [23,24]. Thus, for a generation G, we define the parameter vectors as

$$\mathrm{x}_G^{(p)} = \left\{ a^{(p)}, b^{(p)}, \mu^{(p)}, \left(\theta_{0,j}^{(p)}, \dot{\theta}_{0,j}^{(p)} \right)_{j=1}^{N} \right\}, \tag{9}$$

where $1 \leq p \leq N_p$, being N_p the population size. As practically all the heuristic methods, DE has control parameters affecting its convergence. These are the crossover constant C_R, the scaling factor F and N_p. Finding a suitable set of these parameters can be a tricky task since they are problem-dependent [25]. We do not adopt any special strategy here, instead we use try and error tactics following some tips from the Refs. [25–27], to find that $C_R = 0.9$, $F = 0.8$ and $N_p \geq 10$ $(3 + 2N)$ produce good convergence in general. The search space is defined as follows: $0 < a < 1$, $0 < b < 1$, $0 < \mu < 0.25$, while θ_0 and $\dot{\theta}_0$ are allowed to vary up to ± 0.1 from the measured value. Convergence of DE is tested by evaluating the difference among the fitness of the best and worst individuals of the population: the calculation stops if this difference is less than 0.001.

Table 1 shows the results of four representative optimization calculations. Certainly, the first thing that comes out is that viscous damping seems to be linear, since all the optimal solutions produce $a \cong 0$. These somewhat surprising result confirms the hypothesis of Horton and coworkers [28], who stated that dissipation in a parametric pendulum can be accurately represented by assuming Coulomb friction and only a linear component of viscous damping (in fact, they obtained a very good representation of transient tumbling chaos by following such hypothesis). A possible explanation for this behavior comes from fluid mechanics. Drag force is proportional to the velocity for a laminar flow, and the squared velocity for a turbulent flow [29]. For a flow past a flat plate, which is the case of our pendulum bob, transition from laminar to turbulent begins at a Reynolds number of the order of 5×10^5 [30]. In our experiment $\mathrm{Re} < 1 \times 5 \times 10^4$, that is a laminar flow, and then it seems logical that quadratic damping to be negligible. However, it cannot be said that the quadratic component of velocity does not influence damping at all, since the dry friction term in Eq. (5) includes a velocity squared. Since modeling damping has proven to be complex [13], the discussion remains open on this point.

Both b and μ do not differ significantly from one calculation to another: $b \in [0.473, 0.622]$ and $\mu \in [0.135, 0.157]$. This is interpreted as an approximately constant behavior, showing that assumptions of Eq. (3)–(4) are reasonable. More calculations were performed for different values of N, experimental data and settings of the shaker, not presented here due to a matter of space. Fig. 3 shows a typical convergence plot of an optimization calculation.

After determining a, b and μ, a validation of the model is performed by comparisons with new experiments. We fix $a = 0$, $b = 0.5$ and $\mu = 0.15$ as representative magnitudes and solve the problem of Eq. (8) with $N = 1$ to determine θ_0 and $\dot{\theta}_0$ of each measurement in question. Then, time histories of $\theta(t)$ and $\dot{\theta}(t)$ are obtained by solving Eq. (5). In the comparative study, we also include simulations using $a = 0$, $b = 0.3$ and $\mu = 0$, being this magnitude of b estimated by the classic method of logarithm decrement, from several free decay tests. To be fair, initial conditions are also determined in this case by solving Eq. (8).

Comparative plots of some time histories are presented in Figs. 4–7. We refer to the simulations as 'Sim. A' or 'Sim. B' if damping parameters obtained by optimization (present approach) or by logarithm decrement, respectively. Fig. 4 corresponds to a rotational response, with a long rotational multi-periodic transient. Both simulations reproduce well the experiment, but Sim. B predicts a period-2 rotation in the long term, while the experiment shows period-1 (this was verified by a Poincaré map, not shown here). In Fig. 5 a rotation with a short oscillatory transient is presented. In this case, Sim. A has an almost perfect agreement, while Sim. B is unable to reproduce the experiments, predicting oscillatory response in the long term. Fig. 6 presents a rotation with a very complex chaotic transient. Both simulations predict rotations as steady state but again Sim. B wrongly predicts period-2 while experiment shows period-1. Transient state is not well modeled in

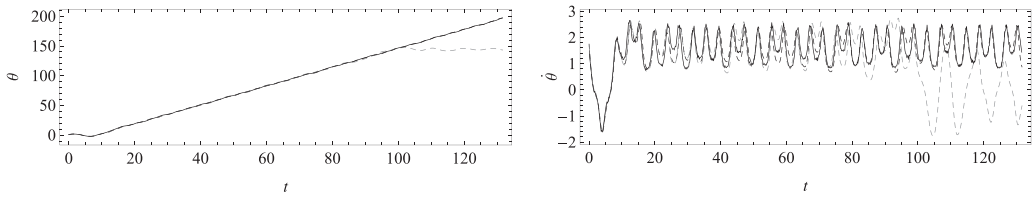

Fig. 5. Comparative plots of experimental and simulated angular position and velocity for $R = 0.694$, $\omega = 1.592$, $\lambda = 0.126$. (–): Experimental. (- -): Simulation A, $a = 0$ ($\alpha = 0$), $b = 0.5$ ($\beta = 0.056$), $\mu = 0.15$ ($M = 0.007$). (_ _): Simulation B, $a = 0$ ($\alpha = 0$), $b = 0.3$ ($\beta = 0.034$), $\mu = 0$ ($M = 0$).

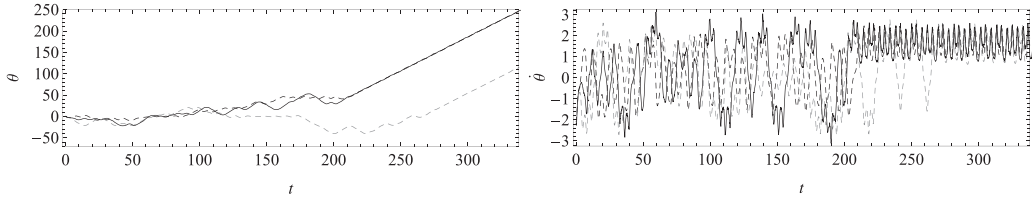

Fig. 6. Comparative plots of experimental and simulated angular position and velocity for $R = 0.700$, $\omega = 1.585$, $\lambda = 0.126$. (–): Experimental. (- -): Simulation A, $a = 0$ ($a = 0$), $b = 0.5$ ($\beta = 0.109$), $\mu = 0.15$ ($M = 0.007$). (_ _): Simulation B, $a = 0$ ($\alpha = 0$), $b = 0.3$ ($\beta = 0.066$), $\mu = 0$ ($M = 0$).

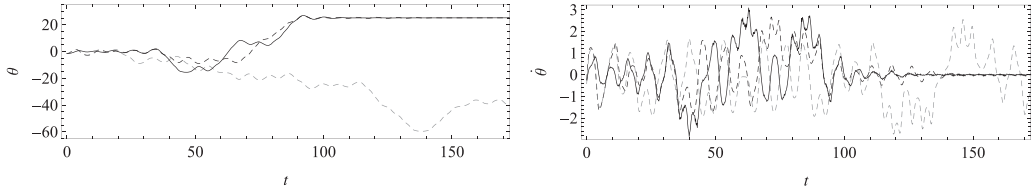

Fig. 7. Comparative plots of experimental and simulated angular position and velocity for $R = 0.694$, $\omega = 1.592$, $\lambda = 0.126$. (–): Experimental. (- -): Simulation A, $a = 0$ ($a = 0$), $b = 0.5$ ($\beta = 0.056$), $\mu = 0.15$ ($M = 0.007$). (_ _): Simulation B, $a = 0$ ($\alpha = 0$), $b = 0.3$ ($\beta = 0.034$), $\mu = 0$ ($M = 0$).

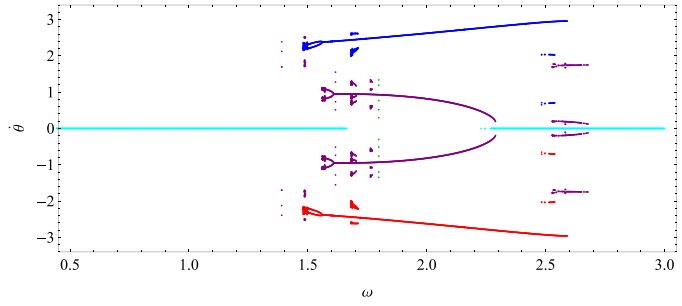

Fig. 8. Bifurcation diagram of the non-dimensional angular velocity for $R = 0.700$, $\lambda = 0.126$. Both viscous and dry friction considered: $a = 0$ ($\alpha = 0$), $b = 0.5$ ($\beta = 0.109$), $\mu = 0.15$ ($M = 0.007$). (•): clockwise rotations, (•): anticlockwise rotations, (•): rest, (•): oscillations, (•): tumbling chaos.

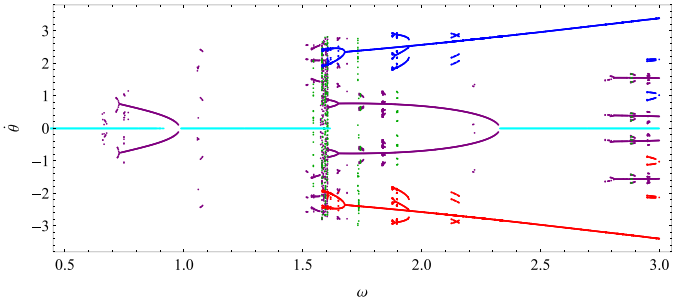

Fig. 9. Bifurcation diagram of the non-dimensional angular velocity for $R = 0.700$, $\lambda = 0.126$. Only linear viscous friction considered: $a = 0$ ($\alpha = 0$), $b = 0.3$ ($\beta = 0.066$), $\mu = 0$ ($M = 0$). (•): clockwise rotations, (•): anticlockwise rotations, (•): rest, (•): oscillations, (•): tumbling chaos.

any case, but Sim. A at least predicts its duration. Sim. B also fails in the prediction of the angular position. The last example, Fig. 7, corresponds to a motion that goes to the vertical hanging position after a chaotic transient. Once again, Sim. A predicts well the steady state but not the transient state, while Sim. B fails noticeably.

Notable differences between Sim. A and B are found while constructing bifurcation diagrams, which show the topology of the responses for a range of a parameter. This can be seen in the examples presented in Figs. 8–9, where ω is varied while the remaining parameters are kept as in the example of Fig. 6. From both plots, it can be clearly seen that if only linear viscous damping is considered as in Fig. 9, a much more complex and unrealistic dynamics is predicted. More importantly from the point of view of energy harvesting is that the existence of rotations can be erroneously estimated, leading to inadequate harvester designs. For example: from the results of Fig. 9, one could design a harvester to work at $2.6 < \omega < 3.0$; but Fig. 8 clearly shows that rotations are not possible at that range in the real-world, and thus the harvester will not be able to work correctly.

6. Conclusions

It is known that damping strongly influences the dynamics of every mechanical system. But maybe due to the complexities of its mechanisms, not much attention has been paid to the topic in recent investigations on energy harvesting from the parametric pendulum. The majority of these studies consider only a viscous damping term linear in velocity [2–11], although this practice has been pointed out as inadequate for real world systems since a long time [12–14].

With this motivation in mind, we conducted a study on damping of the parametric pendulum, with a view on energy harvesting from rotating motion. A model is introduced for such purpose, including a realistic description of pendulum damping. Both linear

and quadratic viscous damping terms are considered, along with a Coulomb's dry friction term. Employing detailed experimental time histories as input, damping parameters of a real system are identified by an optimization calculation. We include also as variables of the optimization problem the initial conditions of those time histories. This must be done to further replicate the experiments because of the sensitivity of nonlinear systems on initial conditions, and some uncertainty in the measurements.

A very good agreement is obtained between experiments and simulations, especially for long term behavior. Oscillatory and rotational transients are also well modeled, but not chaotic transients. Of course, this may happen while trying to model chaotic motion with an ideal model in terms of lubrication, temperature, alignment and wear.

The results of our investigations demonstrate that a much better representation of experimental time histories is obtained by using the present damping model than a classic linear model [28]. It is shown that if only linear viscous damping is considered, a much more complex dynamics is predicted, which may not exist in real systems. Besides, linear models fail in the prediction of rotation zones in the bifurcation diagrams. This is crucial for energy harvesting purposes, since the design process of harvester devices is strongly influenced by the correct estimation of those zones.

Acknowledgements

The authors thank the support of CONICET, Secretary of Science and Technology of UTN and Engineering Department of UNS, the valuable advices of Engineer Claudio Gatti and technical assistance of Engineer René Molina at the Mechanical Engineering Department of UTN-FRBB.

References

[1] M. Wiercigroch, A new concept of energy extraction from waves via parametric pendulor. UK patent application, (2010).
[2] K. Nandakumar, M. Wiercigroch, A. Chatterjee, Optimum energy extraction from rotational motion in a parametrically excited pendulum, Mech. Res. Commun. 43 (2012) 7–14.
[3] D. Yurchenko, P. Alevras, Dynamics of the N-pendulum and its application to a wave energy converter concept, Int. J. Dyn. Control 1 (4) (2013) 290–299.
[4] A. Najdecka, S. Narayanan, M. Wiercigroch, Rotary motion of the parametric and planar pendulum under stochastic wave excitation, Int. J. Nonlin. Mech. 71 (2015) 30–38.
[5] F. Reguera, F.E. Dotti, S.P. Machado, Rotation control of a parametrically excited pendulum by adjusting its length, Mech. Res. Commun. 72 (2016) 74–80.
[6] T. Andreeva, P. Alevras, A. Naess, D. Yurchenko, Dynamics of a parametric rotating pendulum under a realistic wave profile, Int. J. Dyn. Control 4 (2) (2015) 233–238.
[7] M.J. Clifford, S.R. Bishop, Rotating periodic orbits of the parametrically excited pendulum, Phys. Lett. A 201 (1995) 191–196.
[8] F.E. Dotti, F. Reguera, S.P. Machado, A review on the nonlinear dynamics of pendulum systems for energy harvesting from ocean waves, in: Proc. of the 1 St PANACM, Buenos Aires, Argentina, 2015, pp. 1516–1529.
[9] S. Lenci, G. Rega, Experimental versus theoretical robustness of rotating solutions in a parametrically excited pendulum: a dynamical integrity perspective, Physica D 240 (2011) 814–824.
[10] S. Lenci, M. Brocchini, C. Lorenzoni, Experimental rotations of a pendulum on water waves, J. Comput. Nonlin. Dyn. 7 (2011) 011007–011071.
[11] A. Najdecka, T. Kapitaniak, M. Wiercigroch, Synchronous rotational motion of parametric pendulums, Int. J. Nonlin. Mech. 70 (2015) 84–94.
[12] R.W. Leven, B. Pompe, C. Wilke, B.P. Koch, Experiments on periodic and chaotic motions of a parametrically forced pendulum, Physica D 16 (1985) 371–384.
[13] P.T. Squire, Pendulum damping, Am. J. Phys. 54 (11) (1986) 984–991.
[14] R.A. Nelson, M.G. Olsson, The pendulum –Rich dynamics from a simple system, Am. J. Phys. 54 (2) (1986) 112–121.
[15] B.J. Miller, More realistic treatment of the simple pendulum without difficult mathematics, Am. J. Phys. 42 (1974) 286–303.
[16] F. Wardle, Ultra-precision Bearings, Elsevier, Amsterdam, 2015.
[17] SKF rolling bearings catalogue. SKF Group, Göteborg, Sweeden, (2013).
[18] S. Lenci, L. Consolini, F. Clementi, On the experimental determination of dynamical properties of laminated glass, Ann. Solid Struct. Mech. 7 (2015) 27–43.
[19] J.L. Cortizo Rodríguez, E. Rodríguez Ordóñez, Elementos de Máquinas. Teoría y Problemas Universidad de Oviedo, Oviedo, Spain, (2010).
[20] H. Olsson, K.J. Astrom, C. Canudas de Wit, M. Gafvert, P. Lischinsky, Friction models and friction compensation, Eur. J. Control 4 (1998) 176–195.
[21] J.L. Meriam, L.G. Kraige, Engineering Mechanics Volume 2–Dynamics, John Wiley & Sons, New York, 1986.
[22] W. Szemplinska-Stupnicka, E. Tyrkiel, A. Zubrzycki, The global bifurcations that lead to transient tumbling chaos in a parametrically driven pendulum, Int. J. Bifurcat. Chaos 10 (9) (2000) 2161–2175.
[23] R. Storn, K. Price, Differential evolution—a simple and efficient heuristic for global optimization over continuous spaces, J. Global Optim. 11 (4) (1997) 341–359.
[24] K. Price, R. Storn, J. Lampinen, Differential Evolution—A Practical Approach to Global Optimization, Springer, Berlin, 2005.
[25] F. Peñuñuri, C. Cab, O. Carvente, M. Zambrano-Arjona, J. Tapia, A study of the classical Differential Evolution control paramerts, Swarm Evol. Comput. 26 (2016) 86–96.
[26] A. Piotrowski, Review on differential evolution population, Swarm Evol. Comput. 32 (2016) 1–24.
[27] R. Storn, On the usage of Differential Evolution for function optimization, in: Proc. of the NAFIPS, Berkeley, USA, 1996, pp. 519–523.
[28] B. Horton, M. Wiercigroch, X. Xu, Transient tumbling chaos and damping identification for parametric pendulum, Phil. Trans. R. Soc. A 366 (2008) 767–784.
[29] G. Falkovich, Fluid Mechanics: A Short Course for Physicists, Cambridge University Press, New York, 2011.
[30] J.W. Elder, The flow past a plate of finite width, J. Fluid Mech. 9 (1) (1960) 133–153.